Astronomy in the Submillimeter and Far Infrared Domains with the Herschel Space Observatory
L. Pagani and M. Gerin (eds)
EAS Publications Series, **34** *(2009) 43–62*
www.eas.org

THE PACS INSTRUMENT

A. Poglitsch[1] and B. Altieri[2]

Abstract. The Photodetector Array Camera and Spectrometer on Herschel provides imaging line spectroscopy and imaging photometry in the 55–210 μm wavelength band. In photometry mode, two filled silicon bolometer arrays with 16×32 and 32×64 pixels, respectively, are used to simultaneously image two bands, 60–85 μm or 85–130 μm and 130–210 μm, over a field of view of $\sim 1.75' \times 3.5'$, with Nyquist beam sampling in each band. In spectroscopy mode, two Ge:Ga photoconductor arrays (stressed and unstressed) with 16×25 pixels, each, are used to image a field of $\sim 50'' \times 50''$, resolved into 5×5 pixels, with a spectral resolution of ~ 175 km s^{-1} and an instantaneous spectral coverage of ~ 1500 km s^{-1}. In both modes the performance is expected to be not far from background-noise limited, with sensitivities (5σ in 1 h) of ~ 4 mJy or $3\text{–}20 \times 10^{-18}$ W/m^2, respectively.
We summarise the design of the instrument and its subunits, describe the observing modes in combination with the telescope pointing modes, report results from instrument level performance tests of the Flight Model, and present our current prediction of the in-orbit performance of the instrument.

1 Introduction

The far infrared and submillimetre satellite Herschel will open up the wavelength range 60–600 μm to photometry and spectroscopy with unprecedented sensitivity and spatial resolution, unobscured by the Earth's atmosphere.

Within the complement of three instruments selected to form the science payload, the shortest wavelength band, 60–210 μm, will be covered by the Photodetector Array Camera & Spectrometer (PACS), which will provide both photometric and spectroscopic observing modes suited to address the key scientific topics of the Herschel mission.

[1] Max-Planck-Institut für Extraterrestrische Physik, Garching, Germany
[2] European Space Astronomy Centre, Villafranca del Castillo, Spain

DOI: 10.1051/eas:0934004

Article published by EDP Sciences

2 Instrument Requirements

The advantage of Herschel in its core wavelength range – compared to missions like Spitzer and SOFIA or ground based facilities – is its unique combination of angular resolution and sensitivity which enables the scientific program foreseen with Herschel. The key science to be addressed with Herschel requires from PACS the provision of diffraction/telescope-limited, broad-band photometric imaging, and of medium-resolution spectroscopic capabilities, at wavelengths from $\sim$60 μm to $>$200 μm. The lower wavelength limit is mainly determined by the optical quality of the Herschel telescope; at shorter wavelengths Herschel will not be able to maintain its advantage over Spitzer in terms of angular resolution.

2.1 Photometer Requirements

Photometric color diagnostics requires spectral bands with a relative bandwidth $\Delta\lambda/\lambda < 1/2$. In coordination with the Spectral and Photometric Imaging Receiver (SPIRE) bands, the PACS photometric bands have been defined as 60–85 μm, 85–130 μm, and 130–210 μm.

A major fraction of the Herschel observing time will go to deep and/or large scale photometric surveys. For these, mapping efficiency is of the highest priority. Mapping efficiency is determined by both, the instantaneous field of view of the instrument (number of pixels) and the sensitivity per pixel. How the two parameters enter into a measure of the mapping efficiency greatly depends on the mapped objects. A main discriminator is the confusion limit (source separation $\sim$ a few beam diameters): if confusion is reached after a reasonably short integration time, then sensitivity per detector can be traded for number of pixels. In the opposite case, the sensitivity per pixel is the more important parameter. Within the PACS bands, the confusion limit in selected fields is expected as low as a few mJy (5σ), and detector sensitivity (if a trade-off turned out necessary) has to get higher priority than number of pixels. Thus, the PACS instrument had to be designed around the largest possible detector arrays affordable without a compromise in sensitivity, *i.e.*, with the highest possible system detective quantum efficiency and telescope background limited noise performance.

Simultaneous observation of – preferably all – photometric bands is also suggested by the need to maximize observing efficiency, and a by-product when detector technology requires different detectors to cover the full PACS wavelength band with optimum sensitivity.

Extraction of very faint sources from the very bright telescope background has to be ensured, by a combination of intrinsic photometric stability and ways to precisely flat-field the system responsvity on as short a timescale as necessary, as well as by spatial modulation techniques (chopping/nodding, on-the-fly mapping).

2.2 Spectrometer Requirements

The key spectroscopic observations ask for the detection of weak spectral lines with medium resolution (R $\sim$ 1500). The sources to be observed may have precisely known positions or, in the case of follow-up observations to the photometric surveys, only within the absolute position error of the Herschel satellite. In any case, the intrinsic uncertainty in the satellite pointing should not compromise the measurement, neither in sensitivity nor in spatial resolution. Subtraction of the high telescope background must be accomplished.

Sensitivity is the most important parameter for optimisation; with background-limited performance the best sensitivity is obtained if the spectrometer fulfills the following conditions: The detection bandwidth must not be greater than the resolution bandwidth, which should be matched to the line width of the source, and the line flux from the source must be detected with the highest possible efficiency in terms of system transmission, spatial and spectral multiplexing.

Wavelength calibration accurate to a fraction of the resolution bandwidth must be ensured for all observations. Intensity calibration and removal of modulations in the spectral response (defringing) must be provided for.

3 Instrument Design and Subunits

The instrument concept has been developed based on the requirements stated above on the one hand, and within the boundary conditions set by the satellite and the available detector technology on the other hand. The instrument will offer two basic modes in the wavelength band 60–210 μm:

- Imaging dual-band photometry (60–85 μm or 85–130 μm and 130–210 μm) over a field of view of $1.75' \times 3.5'$, with full sampling of the telescope point spread function (diffraction/wavefront error limited).

- Integral-field line spectroscopy between 57 and 210 μm with a resolution of $\sim$175 km s^{-1} and an instantaneous coverage of $\sim$1500 km s^{-1}, over a field of view of $47'' \times 47''$.

Both modes will allow spatially chopped observations by means of an instrument-internal chopper mirror with variable throw; this chopper is also used to alternatively switch two calibration sources into the field of view.

The focal plane sharing of the instrument channels is shown in Figure 1. The photometric bands, which can be observed simultaneously, cover the same field of view, while the field of view of the spectrometer is offset from the photometer field (Fig. 1). Since photometry and spectroscopy operation are mutually exclusive this has no effect on the observing efficiency. The focal plane unit provides these capabilities through five functional units:

- common input optics with the chopper, calibration sources and a focal plane splitter,

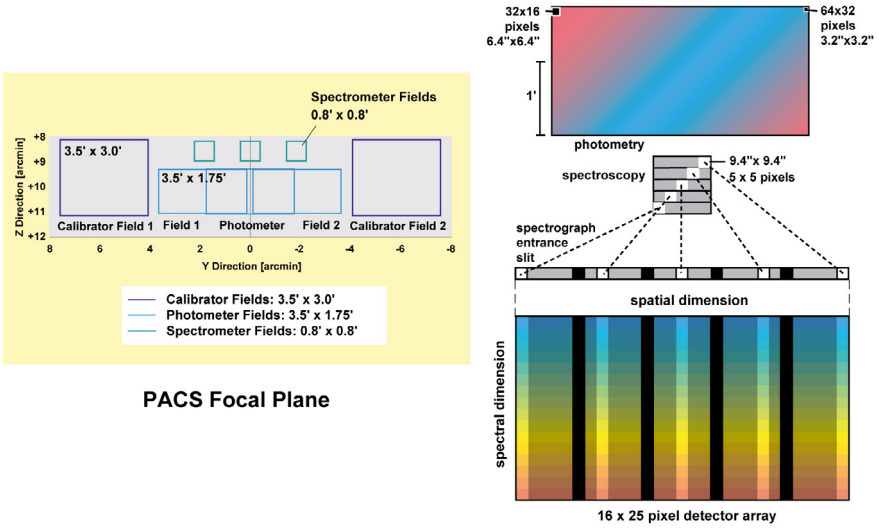

Fig. 1. *Left*: PACS focal plane usage. Long-wavelength and short-wavelength photometry bands cover identical fields of view. The spectrometer field of view is offset in the -z direction. Chopping is done along the y axis (left-right in this view) and also allows observation of the internal calibrators on both sides of the used area in the telescope focal plane. The chopper throw for sky observations is $\pm 1/2$ the width of the photometer field such that object and reference fields can be completely separated (photometer field 1 and 2). *Right*: focal plane footprint. A fixed mirror is used to split the focal plane into the photometry and spectroscopy channels of the instrument. In the photometry section, the two wavelength bands are simultaneously imaged with different magnification to reach full beam sampling in both bands. In the spectroscopy section, an optical image slicer re-arranges the 2-dimensional field along the entrance slit of the grating spectrograph such that, for all spatial elements in the field, spectra are observed simultaneously.

- a photometer optical train with a dichroic beam splitter and separate re-imaging optics for the short-wavelength bands (60–85 μm/85–130 μm) and the long-wavelength band (130–210 μm), respectively; band-defining filters on a wheel select one of the two short-wavelength bands at a time,

- a spectrometer optical train with an image slicer unit for integral field spectroscopy, an anamorphic collimator, a diffraction grating in Littrow mount with associated actuator and position readout, anamorphic re-imaging optics, and a dichroic beam splitter for separation of diffraction orders,

- 2 bolometer arrays with cryogenic buffers/multiplexers and a common 0.3 K sorption cooler,

- 2 photoconductor arrays with attached cryogenic readout electronics (CRE).

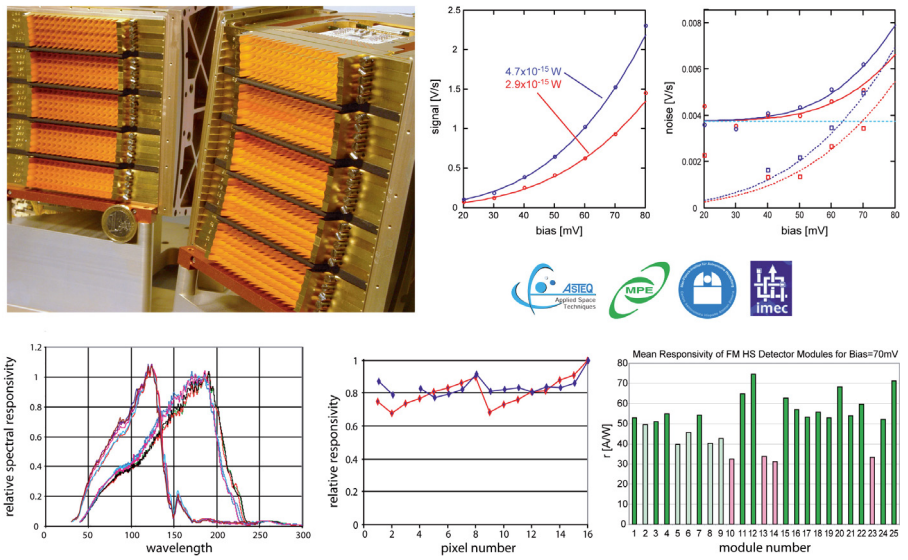

Fig. 2. *Top left*: fully assembled 25 × 16 stressed (back) and unstressed (front) Ge:Ga photoconductor arrays with integrated cryogenic readout electronics. Top center: Measured (circles) and modeled (lines) detector signal as a function of applied bias voltage for two representative levels of incident light power. *Top right*: noise as a function of bias for the two power levels. The circles represent the measured noise. From the bias- and power dependence of the noise one can decompose the noise into a (constant) contribution from the readout electronics (dashed horizontal line) and the photon background noise. The solid lines represent the total noise model. The squares mark the "measured" photon noise obtained by subtracting the derived readout noise from the measured total noise, for comparison with the pure photon noise model (dotted lines). The main free parameter in the model fit is the quantum efficiency of the detector. *Bottom left*: relative spectral response of stressed (long wavelength) and unstressed (short wavelength) detectors. *Bottom center*: relative photometric response of pixels within modules. *Bottom right*: absolute photometric mean response of the 25 modules used for the high-stress flight model array. The modules with the lowest responsivity have been placed in the four corners of the field of view.

A detailed description of the instrument and its subunits would be beyond the scope of this article; we refer the interested reader to the literature (Poglitsch *et al.* 2003; Poglitsch *et al.* 2004) and present only the two major enabling-technology developments for this instrument, which are its detectors.

3.1 Photoconductor Arrays

The 25 × 16 pixels Ge:Ga photoconductor arrays (Fig. 2) are a completely modular design. 25 linear modules of 16 pixels each are stacked together to form a contiguous, 2-dimensional array. The light cones in front of the actual detector block

provide for area-filling light collection in the focal plane. Details of the design of both arrays have been published (Kraft *et al.* 2000; Kraft *et al.* 2001; Rosenthal *et al.* 2002; Poglitsch *et al.* 2003).

Responsivity measurements of both stressed and unstressed modules show sufficiently homogeneous spectral and photometric response within each module and between modules (Fig. 2, bottom center/right). Absolute responsivity numbers are preliminary as the optimum bias for in-orbit operation is not determined, yet. Likely numbers will be ∼10 A/W for the unstressed detectors and ∼40 A/W for the stressed detectors.

Each linear module of 16 detectors is read out by a cryogenic amplifier /multiplexer circuit (CRE) in CMOS technology (Charlier 2000; Creten *et al.* 2002). The readout electronics is integrated into the detector modules.

Measurements on FM detectors have been carried out to optimize their operation and to allow a prediction of their in-orbit performance. Some of these measurements were suited to separate the readout electronics noise from the intrinsic photon detection process (Fig. 2, top center/right). These measurements can be consistently described by a constant contribution in current noise density from the CREs and a noise component proportional to the photon background noise, where this proportionality can be expressed in terms of an (apparent) quantum efficiency, with a peak value of 26%. This number may seem low; yet, the much lower noise of these detectors makes them a better choice than the bolometers described next, which have a higher detection efficiency, but much more noise, and are thus ruled out for use in the spectrometer with its low background flux per detector.

3.2 Bolometer Arrays

The PACS bolometers are filled arrays of square pixels which allow instantaneous beam sampling. 4×2 monolithic sub-arrays of 16×16 pixels are tiled together to form the short-wave focal plane array (Fig. 3, top center). In a similar way, 2 subarrays of 16×16 pixels are tiled together to form the long-wave focal plane array. The subarrays are mounted on a 0.3 K carrier which is thermally isolated from the surrounding 2 K structure. The buffer/multiplexer electronics is split in two levels; a first stage is part of the indium-bump bonded back plane of the focal plane arrays, operating at 0.3 K. Ribbon cables connect the output of the 0.3 K readout to a buffer stage running at 2 K. The multiplexing readout samples each pixel at a rate of 40 Hz or 20 Hz. Details on the bolometer design can be found in (Agnese *et al.* 1999; Agnese *et al.* 2003; Simoens *et al.* 2004; Billot *et al.* 2007). Both array assemblies are mounted in a subunit of the FPU (Fig. 3, top right) together with the 0.3 K cooler (Duband & Collaudin 1999) which provides uninterrupted operation for two days, with a typical hold time of 59 hours measured in our lab cryostat. The post-detection bandwidth (thermal/electrical) of the bolometers is ∼3 Hz; the noise of the bolometer/readout system has a strong 1/f component such that a clear 1/f "knee" frequency cannot be defined (Fig. 3, bottom right). We (somewhat arbitrarily) assume a factor of ten in post-detection frequency

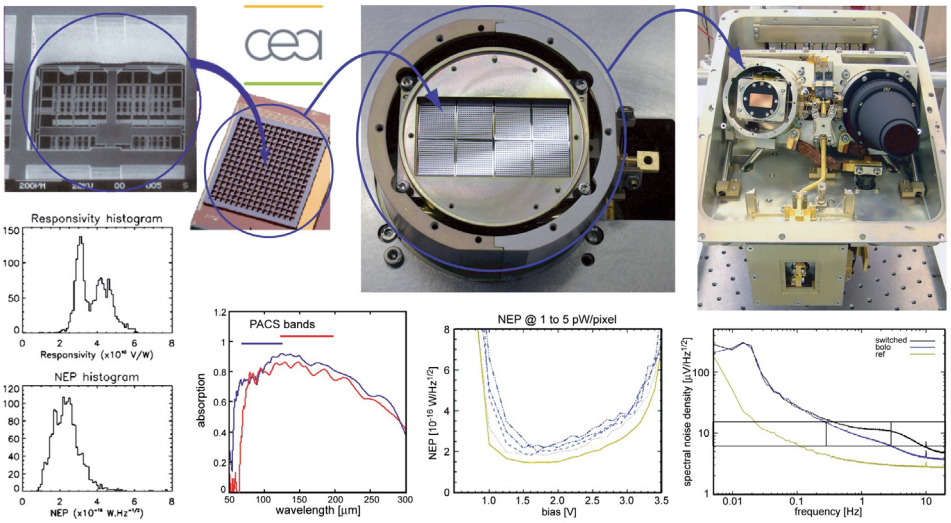

Fig. 3. *Top left*: micrograph of one pixel of the filled bolometer array next to a photo of a 16 × 16 pixels subarray. The physical size of a PACS pixel is 0.75 mm. The absorber and back-reflector grids as well as the integrated thermistor are monolithic silicon structures. Top centre: 4 × 2 subarrays form the focal plane of the FM short-wave bolometer assembly. The 0.3 K focal plane is suspended from its 2 K enclosure by Kevlar strings. Close to the right edge of the picture, the thermal interface to the 0.3 K cooling bar is visible. *Top right*: photometer focal plane unit (FM) with the two bolometer assemblies (short-wave, baffle cone removed / long-wave, with baffle cone) and the 0.3 K sorption cooler. A Kevlar-suspended cooling bar provides the thermal connection from the cold tip of the cooler to the 0.3 K interfaces of the bolometer assemblies. *Bottom left*: responsivity and NEP histograms of the short-wave bolometer array under nominal background illumination. *Bottom centre-left*: efficiency of the short-wave and long-wave bolometer absorber structures. The horizontal bars mark the wavelength ranges of the PACS bands. *Bottom centre-right*: NEP as a function of detector bias for a range of background levels. *Bottom right*: electrical noise spectra of the bare multiplexer (*bottom*) and of the detector/multiplexer in simple readout mode (*middle*) and in "double-correlated" readout mode (*top*).

(*i.e.*, 0.3 Hz – 3 Hz) to be sufficient to cover both, chopped and continuously scanned observations, and consider the noise in this band as relevant for sensitivity estimates. Measurements of the bolometer NEP as a function of electrical bias for a range of background loads (Fig. 3, bottom center-right) show that there is a relatively broad minimum in NEP whose position is almost independent of the incident power over the range estimated for the Herschel telescope. In-orbit optimization should, therefore, be uncritical; if the telescope background turned out considerably less than nominal, there would be a small, but significant gain in sensitivity. The efficiency of the absorber structures designed for the "red" and "blue" arrays (Fig. 3, bottom center-left) was, in fact, found best over both

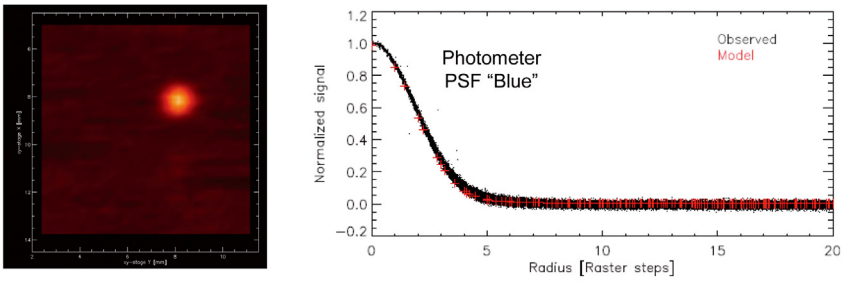

Fig. 4. Measurement of the photometer PSF in the 70 μm band. The source was a hole mask, which was scanned across the field of view in 1/3 pixel steps. The left panel shows the image of the scanned source as seen by one pixel. The right panel shows a radial cut of the PSF obtained from all pixels. The central peak appears slightly wider than the model (red crosses), but there is no indication of unexpected large scale wings.

wavelength bands for the "blue" design; therefore, it has been used for all subarrays in the FM focal planes. The responsivity, particularly between subarrays, varies considerably (Fig. 3, bottom left, upper panel), but the readout electronics has been adjusted accordingly, and the NEP distribution (Fig. 3, bottom left, lower panel) is not affected by this.

4 Test Results

A wide range of tests has been performed on components, subunits, and the full instrument in order to characterise and calibrate the instrument under flight-representative conditions, as much as possible, on ground. We present results with the most direct impact on the performance of the instrument.

4.1 Instrument Point Spread Function

Measurements of the instrument PSF were performed in all three photometric bands as well as in both branches of the spectrometer. The telescope simulator used for the instrument level tests has a significantly smaller wavefront error than the Herschel telescope specification. We expect a very similar PSF in orbit; the wavefront error of the telescope is expected to be small enough that it will mostly lead to some loss of power in the central peak of the PSF but not significantly increase its width.

4.1.1 Photometer Point Spread Function

Measurements of the photometer PSF in the 70 μm band, done with a pinhole source at the entrance to our telescope simulator optics, are shown in Figure 4. This is the most critical band since it should deliver the narrowest PSF.

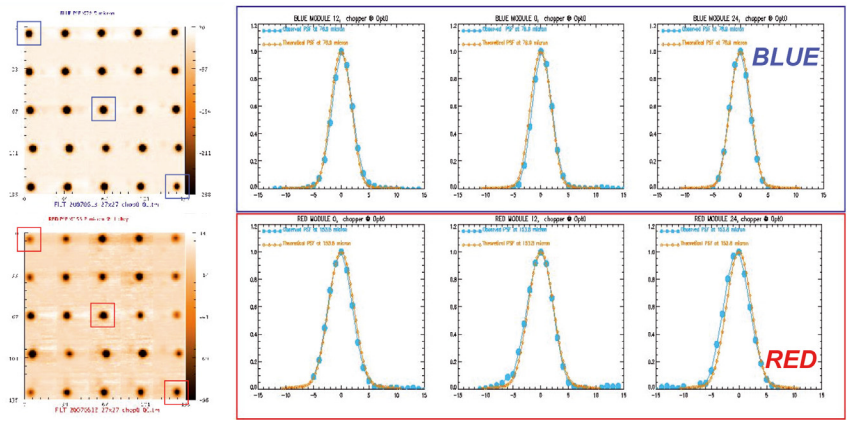

Fig. 5. Measurement of the spectrometer PSF in the "blue" and "red" branches. The source was a hole mask, which was scanned across the field of view in 1/3 pixel steps. The left panels show the (spectrally collapsed) images of the scanned source as seen by each spatial pixel. The right panels show cuts through three selected pixels, as indicated by the boxes in the left panels, in both spectrometer branches. Measured PSFs agree well with the model prediction.

The measurements in all three bands agree well with the predicted profiles based on a convolution of the pinhole source with the diffraction by the optics and the pixel size.

4.1.2 Spectrometer Point Spread Function

Measurements of the spectrometer PSF in the "blue" and "red" branches, done with a pinhole source at the entrance to our telescope simulator optics, are shown in Figure 5. Since the source had no spectral features, each of the 5×5 spatial elements in our field of view has been spectrally collapsed, to increase the signal-to-noise ratio.

The measurements in all three bands agree well with the predicted profiles based on a convolution of the pinhole source with the diffraction by the optics and the pixel size.

4.2 Filter Efficiency

The filters used in PACS in transmission or reflection have been measured individually in our FTS before integration. The optical efficiencies of the entire filter chains have then been calculated by multiplying the individual filter efficiencies. The spectrometer filter chain efficiencies are shown in Figure 6, the photometer band efficiencies, obtained by multiplying all filter efficiencies and the bolometer efficiency in each band, are shown in Figure 9.

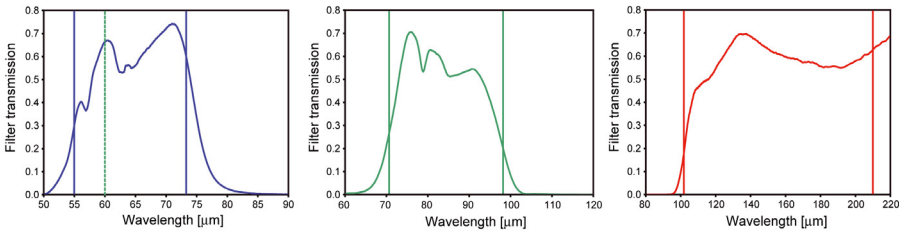

Fig. 6. Filter transmission of the spectrometer filters. The graphs represent the overall transmission of the combined filters in each branch of the instrument. The nominal band limits are indicated by the vertical lines. Left: 55–73 μm spectrometer band. This filter band was desigend for use in the third grating order, but can be used in the "extended second order" mode down to 60 μm, as indicated by the dashed line. Centre: 71–98 μm spectrometer band (second order). Right: 102–210 μm spectrometer band (first order). Note: Tolerances intrinsic to the filter manufacturing process have led to an effective gap in wavelength coverage between 98 and 102 μm.

5 System Performance Prediction

Based on the results from the Instrument Level Tests and our tests of FM components/subunits and our present knowledge of the Herschel satellite, the performance of the entire system can be predicted through a detailed instrument model.

The system sensitivity of the instrument at the telescope depends mainly on the optical efficiency, *i.e.* the fraction of light from an astronomical source arriving at the telescope that actually reaches the detector, on the photon noise of the thermal background radiation from the telescope or from within the instrument, and on detector/electronics noise.

5.1 Optical Efficiency

The system optical efficiency has been modeled to the following level of detail:

- *Telescope efficiency*: The fraction of the power of a point source in the central peak of the point spread function is modeled in terms of absorption/obstruction, diffraction, and geometrical wave front errors (6 μm r.m.s.), which have been assumed to occur as spherical aberration.
- *Chopper*: Errors/jitter in the chopper throw and the duty cycle (>80%) are considered.
- *Mirrors and filters*: Scatter/absorption losses – excluding diffraction – on each reflection by a mirror (1%) and efficiencies of filters/dichroics (as measured for the FM filters individually) are taken into account.
- *Diffraction*: An end-to-end diffraction analysis with the physical optics package GLAD 4.5 has been carried out for the spectrometer, where the image

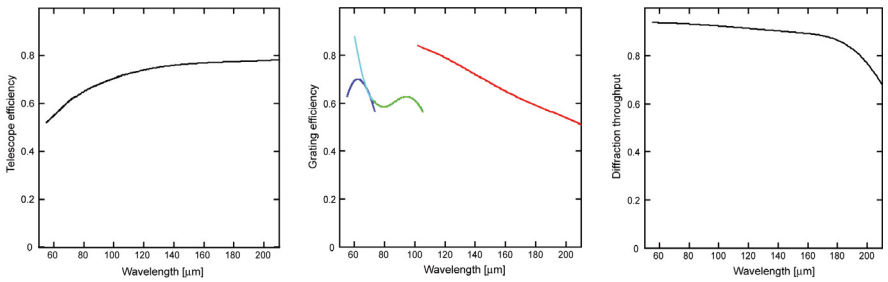

Fig. 7. Optical efficiencies. *Left*: telescope (main beam) efficiency for an assumed wave front error of 6 μm r.m.s. *Center*: calculated grating efficiency. *Right*: diffraction throughput of the spectrometer optics; the diffraction losses mainly occur in the image slicer.

slicer is the most critical element of the PACS optics (Poglitsch *et al.* 1999; Looney *et al.* 2003), and a simplified analysis for the less critical photometer as well as the effect of diffraction/vignetting by the entrance field stop and Lyot stop have been included.

- *Grating efficiency*: The grating has been analysed and optimised with a full electromagnetic code (Poglitsch *et al.* 1999); the validity of this code has been confirmed by FTS measurements on a grating sample made by the manufacturer of the FM grating.

5.2 Detectors

The NEP of the Ge:Ga photoconductor system is calculated over the full wavelenegth range of PACS based on the CRE noise and peak quantum efficiency determination at detector module level for the high-stress detectors. For the low-stress detectors we assume the same peak quantum efficiency. The quantum efficiency as a function of wavelength for each detector can be derived from the measured relative spectral response function. Instrument level test results at one exemplary wavelength in each spectrometer channel are shown in Figure 8. It is interesting to note that the performance of the "blue" channel is significantly better than expected. We attribute this to an overestimate of the readout electronics noise based on our measurements at subunit level, which were performed with different electronics than the flight electronics. The achievable in-orbit performance depends critically on the effects of cosmic rays, in particular, high-energy protons. We have performed proton irradiation tests at the synchrotron source of the Université Catholique de Louvain (Louvain la Neuve, Belgium) on stressed and unstressed detector modules under reasonably realistic conditions in terms of proton flux and energy, FIR background, and metallic shielding by the cryostat. A preliminary analysis of the results indicates that, with optimized detector bias settings and modulation schemes (chopping + spectral scanning), NEPs close to those measured without irradiation can actually be achieved (Katterloher *et al.* 2006); we, therefore, make the optimistic assumption that this will also apply to the actual conditions encountered in space.

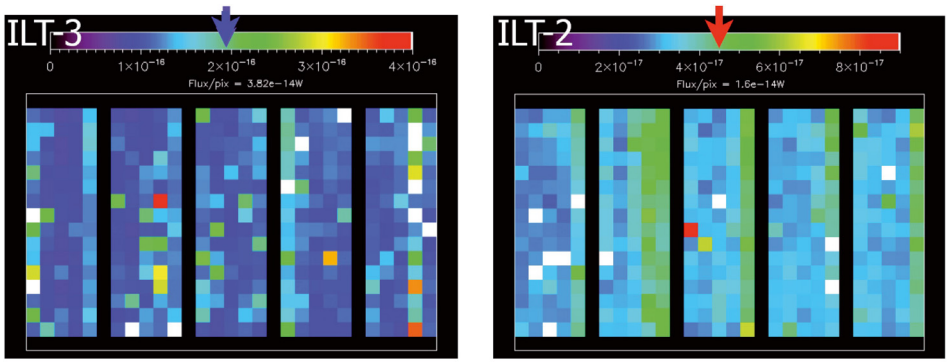

Fig. 8. Spectrometer system NEP maps, referred to the entrance plane of PACS, at exemplary wavelengths for the "blue" (*left*) and "red" detector arrays. The arrows mark the NEP predicted by the instrument model, based on component-level measurements of all elements in the chain. While the performance of the "red" channel is as predicted, the NEP in the "blue" channel seems systematically lower, *i.e.* better, than predicted.

For the bolometers, we have measured "end-to-end" system NEPs in all three photometer bands during the instrument level tests for both, the "blue" and "red" focal planes under realistic photon background.

5.3 System Sensitivity

For the calculation of the system sensitivity we have included our present best knowledge of all components in the detection path as described above. The results for photometry and spectroscopy are shown in Figures 9 and 10.

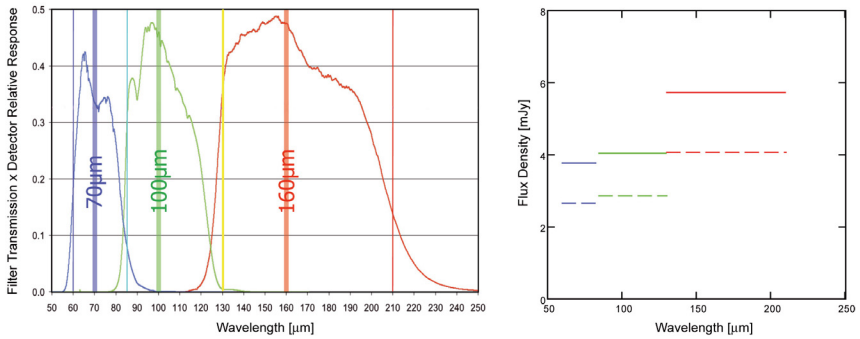

Fig. 9. Effective spectral response of the filter/detector chain (*left*) and sensitivity (5σ/1 h of integration) of PACS on Herschel for point source detection in photometry mode (*right*). The solid lines represent chopped observations where only half of the integration time is spent on the source. The dashed lines represent modulation techniques like on-array chopping or line scans where the source is on the array all the time.

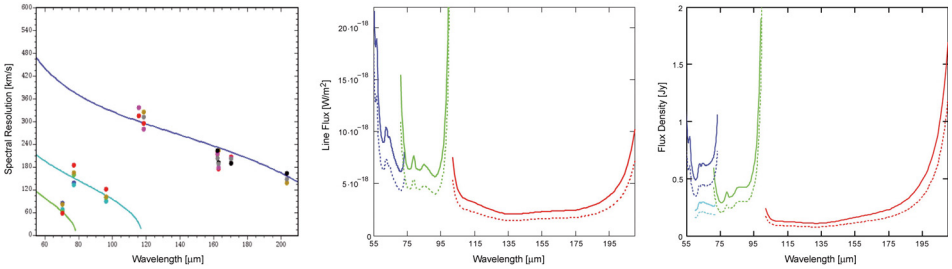

Fig. 10. Spectral resolution as predicted and verified at several, selected wavelengths (*left*) and sensitivity (5σ/1 h of integration) of the PACS instrument on Herschel for point source detection in spectroscopy mode (*right*). For spectroscopy we distinguish between line detection, where we assume that the astronomical line is unresolved at the respective resolving power of the instrument (*center*), and continuum detection where the quoted sensitivity is reached for each spectral resolution element over the instantaneous spectral coverage of the instrument. The solid lines represent chopped observations where only half of the integration time is spent on the source. The dashed lines represent modulation techniques like on-array chopping or line scans where the source is on the array all the time.

It needs to be stressed that these figures must be considered somewhat preliminary, since the instrument level tests of the Flight Model could not fully mimic the satellite environment. In some areas (*e.g.* "red" bolometer detector) we may foresee some improvement compared to the achieved performance used in the system model, in other areas, in particular, the behaviour of the photoconductors under cosmic ray irradiation in the Herschel cryostat, predictions seem less reliable, and more severe adjustments of the sensitivity may occur after the satellite has reached its orbit. The numbers presented here do not contain satellite/AOT overheads, *e.g.*, for slewing, calibration times, or additional "penalties". Exact numbers, therefore, can only be obtained through the HSPOT observing time calculator.

6 Observing with PACS

6.1 AOT concept

Either the photometer or the spectrometer will be used during dedicated Observation Days (OD) of 21 hours. The reason for this is to allow uninterrupted observations with the photometer to optimize the time spent on recycling the photometer cooler, which takes about 2 hours, during a daily telecommunication period of 3 hours per day. As the hold time of the cooler will probably be more than 48 hours, the photometer might even be used for two consecutive ODs.

The Herschel observations are organized around standardized observing procedures, called AOTs (for Astronomical Observation Template). Four different AOTs have been defined and implemented to perform astronomical observations with PACS: two for the spectrometer, one generic for photometry/mapping with

the photometer and having both SPIRE and PACS observing in parallel with their respective photometers.

The PACS AOTs, whether with the photometer or the spectrometer follow a similar pattern of events, preparation of observation, internal calibration and sky observations.

While slewing to the demanded celestial coordinates, PACS is commanded from stand-by mode to photometer set-up or spectrometer set-up ready for operations. After the transition is accomplished, PACS enters into an internal calibration sequence, using the Internal Calibration Sources (ICS) and the data flow is started. Since the calibration is performed while slewing, an otherwise "wasted" time is being profitably used. Currently, the user is "charged" a flat rate of 3 minutes to account for the slew time, regardless of its actual duration.

At regular intervals during the "science" observation, the spacecraft will remain idle while PACS repeats the ICS based calibration.

PACS is commanded back to the relevant standby mode at the end of the observation and the data flow is stopped.

6.2 Spectrometer AOTs

Two different observation schemes are offered with the PACS spectrometer: line and range spectroscopy.

- line spectroscopy mode: a limited number of relatively narrow emission or absorption lines can be observed for either a single spectroscopic FOV ($0.78' \times 0.78'$) or for a larger map. Background subtraction is achieved either through standard chopping/nodding, for faint/compact sources, or through "wavelength-switching" techniques for line measurement of the grating mechanism of bright extended sources.
- range spectroscopy mode: this is a more flexible and extended version of the line spectroscopy mode, where a freely defined wavelength range is scanned by stepping through the relevant angles of the grating, synchronized with the chopper. Both arrays are used at a time.

6.2.1 Line Spectroscopy

This AOT is intended to observe one or several unresolved or narrow spectral line features, on fixed wavelength range of about 1 micron (but varying from 0.35 to 1.8 μm depending on the wavelength and the grating order).

Only lines in the first (102–210 μm) and second order (73–98 μm), or first and third order (55–73 μm) can be observed within a single AOR, to avoid filter wheel movements. If lines of second and third grating order are to be observed on the same target at the same time, two AORs shall be concatenated. Depending on the requested wavelength/grating order, only the data of one of the two detector arrays is normally of interest to the observer.

The fixed wavelength and its immediate neighborhood is observed for each chopper and grating position. For improved flat-fielding, especially for long integrations, the grating is scanned by a number of discrete steps around a specified

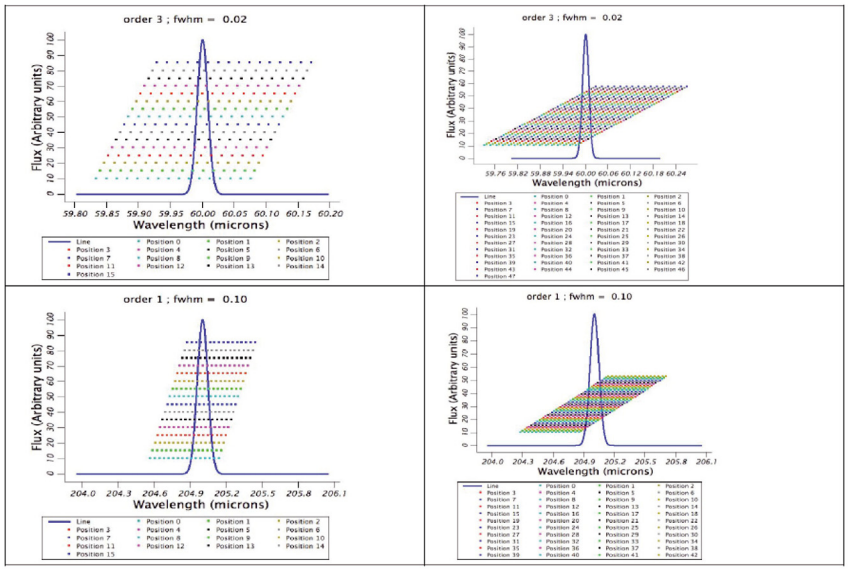

Fig. 11. Visualization of the line scan AOT on an unresolved PACS line (here given by a Gaussian). The grating step used is the nominal one currently coded in AOT design. The left-hand side shows results for 16 grating steps (bright lines chopping-nodding mode case) the right-hand side shows the same for nominal grating positions (standard "faint lines" chopping-nodding) with 48 grating steps. Top row is for a blue line at 60 μm; bottom row is for a red line at 205 μm.

centre position such that drifts in the detector responsivity between individual pixels are eliminated. The principle of line spectroscopy is illustrated in Figure 11.

These grating scans provide for each line and for each of the 5 by 5 spatial pixels a short spectrum with a resolving power of 1700 in its highest resolution covering 1500 km s^{-1} but dependent on the wavelength and order.

Up to 10 lines can be studied within one observation. The relative sensitivity between the lines is controlled by using the line repetition factor, in the line editor of the "wavelength settings" in HSpot, that allows to repeat a line scan several times. While the absolute sensitivity is controlled by the repetition factor in the "observing mode settings", by dedicating a larger amount of time to this observation by increasing the number of nod cycles.

Background subtraction is achieved either through standard chopping/nodding (for faint/compact sources) with a selected chopper throw of 1, 3 or 6 arcmin, or through "frequency-switching" techniques (for line measurements of bright extended sources) of the grating mechanism in combination with the mapping mode. The mapping mode can also be used in chopping/nodding but the map size is then limited to 6 arcmin (the larger chop throw) to avoid chopping into the map itself. Two flavors of the chopping/nodding are available: a default one with 48 grating steps up and down and a faster version for bright lines only with 16 steps.

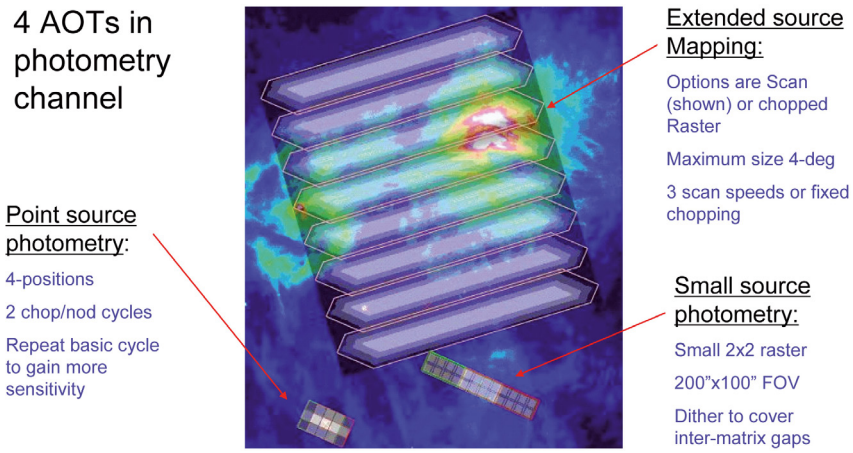

Fig. 12. Visualization of the 4 photometer AOTs (courtesy NHSC).

6.2.2 Range Spectroscopy

Similarly to the line scan spectroscopy mode, this AOT allows to observe one or several spectral line features (up to ten), but the user can freely specify the explored wavelength range.

This AOT is mainly intended to cover rather limited wavelength ranges up to a few microns in high sampling mode (see below) to study broad lines (larger than a few hundreds $\mathrm{km\,s^{-1}}$), which wings would not be covered sufficiently in Line Spectroscopy AOT, or a set of closed lines.

The Range Spectroscopy AOT is also intended to cover larger wavelength ranges up to the entire bandwidth of PACS (in SED mode) in lower sampling density mode, otherwise integration times get quickly prohibitive. In this mode a given wavelength is seen only by two spectral pixels. However the thrust of the spectrometer resides in its high spectral resolution rather than continuum sensitivity.

The use of the chopping/nodding is imposed by the design of the AOT, except in mapping mode where instead an off position can be defined if chopping/nodding is de-selected. In this case only chopping is performed on one of the calibration source and the background subtraction shall be done with OFF position. The chopping/nodding uses the same pattern as in line spectroscopy, with a 3-positions chopping/nodding and same chopper throws to eliminate inhomogeneities in the telescope and sky background. As in line spectroscopy, only ranges in first (102–210 μm) and second order (71–98 μm), or first and third order (55–73 μm) are allowed within a single AOR.

6.3 Photometer AOT

Four generic observing modes are offered to observe with the photometer (Fig. 12).

In all modes the readout frequency of the detectors is 40 hz, but an on-board averaging for 4 frames is performed on-board to keep the allowed averaged telemetry downlink rate within 130 kb/s.

The first three pointed and raster modes make use of chopping at a frequency of 1.25 Hz (*i.e.* 4 averaged frames per chopper plateau), to remove the high telescope background and mitigate the effect 1/f noise and detector gain drifts. While in scan mapping mode the modulation is provided by the spacecraft motion, hence no chopping is applied.

6.3.1 Point-Source Mode

Point-source photometry: This mode is devoted to target isolated and point-like sources or smaller than one blue matrix. A typical use of this mode is for point-source photometry.

It makes use of a classical 4-positions on-array chopping, with dithering option, along the Y-axis combined with nodding along the Z-axis to compensate for the different optical paths. The chopper is used to alternate the source between the left and right part of the array, and the satellite nodding is used to alternate it between the top and bottom part of the array, so that the target is always on the array.

To achieve photometry of fainter sources, the number of nod cycles is increased with the "repetition factor" in the "observing mode settings" to improve the sensitivity and reach fainter flux levels. The sensitivity scales with the inverse of the square root of integration time and repetition factor.

The minimal observing time is about 5.5 mn with a predicted point-source sensitivity of 15–20 mJy (5σ)

6.3.2 Small-Source Mode

Small source photometry: this mode is devoted to target sources that are smaller than the array size, yet larger than a single matrix. To be orientation independent, this means sources that fit in circle of 1.5 arcmin diameter. This mode uses also chopping and nodding, but this time the source cannot be kept on the array at all times.

In this mode, a small 2×2 raster with small step size (17 arcsec) is performed to observe the target, with a classical 3-positions chopping/nodding for each raster position, spending 1 minute on each raster position(both on the nod-on and nod-off). Therefore only half of the science time is actually used for on-source integration, in contrast to the point-source photometry observing mode. With the pattern of gaps between matrices, the 2×2 raster map allows to recover the signal lost between pixels This offers also the advantage of a larger fully-covered area. The parameters of this raster (*i.e.* the displacement in both directions, nod and chop throws) are fixed and not left to the observer's choice.

The minimal observing time is about 15 mn with a predicted point-source sensitivity of 10–15 mJy (5σ).

6.3.3 Raster Mode

In raster mapping the spacecraft goes through a rectangular grid of pointing in instrument reference frame, spending 1 minute per raster position, and chopping by one full array (3.5 arcmin) along the long axis of the detector.

It is intended to cover a limited area in the sky up to $15' \times 15'$. The sensitivity of the map is adjusted by the number of map repetitions.

6.3.4 Scan Mode

The scan mapping is the default mode to cover large areas in the sky for galactic as well as extragalactic surveys. Scan maps are performed by slewing the spacecraft at a constant speed (10, 20 or 60 arcsec/s) along parallel lines, without chopping, the signal modulation being provided by the spacecraft motion.

The highest speed (default value) is envisaged for galactic surveys only, with a significant degradation of the PSF due to the on-board averaging of 4 frames (final 10 Hz sampling). The slow scan speed shall be used for extragalactic surveys, it allows to cover 1 square degree area in about three hours. The PSF degradation and smearing due to the scanning should be almost negligible with the two lowest scan speeds, according to simulations.

Two scan maps of the same area with orthogonal coverage shall be performed to mitigate the stripping effects of the 1/f noise in order to recover extended emission PACS scan maps can be performed either in the instrument reference frame or in sky coordinates.

In all photometer observing modes, dual-band imaging observations are performed, either in the blue (70 μm) and red (160 μm) bands or in the green (100 μm) and red (160 μm) bands, via the a selection button in the main AOT panel.

6.4 SPIRE/PACS Parallel Mode

In parallel mode PACS and SPIRE are operating in photometry mode simultaneously, carrying out large-area mapping observations. PACS is taking data in its red band (130–210 μm) and in one of the blue bands (60–85 μm or 85–130 μm) while SPIRE is observing in its three photometric bands (250, 350 and 500 μm).

The SPIRE/PACS parallel Mode has its own Astronomical Observing Template (AOT), its own user interface in HSpot and the two instruments are operated in a way that the spacecraft infrastructure is optimally used.

Simultaneous observations in five bands are made possible at the expense of slight degradation in instrument performance. The PACS instrument has to apply a higher science data compression ratio with respect PACS prime operations in order to make sure the increased data rate in five bands is still within the allowed limits. The compression ratio is still not precisely known but some loss of sensitivity and spatial resolution is expected. In the first order this is due to the beam smearing effect along the scan direction when bolometer readouts are averaged on-board Herschel.

Two scan speeds are offered: 60″/s and 20″/s with an estimated sensitivity of 150 mJy and 55 mJy (5-sigma) respectively at 100 μm, allowing to cover several square degrees in a few hours.

More details and updated information of AOTs can be found in the PACS Observer's Manual on-line on the Herschel Science Operations web site

(http://herschel.esac.esa.int)

References

Agnese P., Buzzi C., Rey P., Rodriguez L., & Tissot J.-L., 1999, in Infrared Technology and Applications XXV, ed. B.F. Andresen and M.S. Scholl, Proc. SPIE, 3698, 284

Agnese P., Cigna C., Pornin J.-L., *et al.*, 2003, in Millimeter and Submillimeter Detectors for Astronomy, ed T. Phillips and J. Zmuidzinas, Proc. SPIE, 4855, 108

Billot N., Agnèse P., Auguères J.-L., *et al.*, 2006, in Space Telescopes and Instrumentation I: Optical, Infrared, and Millimeter, ed. J.C. Mather, Proc. SPIE, 6265, 9B

Charlier O., 2000, in UV, Optical, and IR Space Telescopes and Instruments, ed. J.B. Breckinridge and P. Jakobsen, Proc. SPIE, 4013, 325

Creten Y., Merken P., Putzeys J., & van Hoof C., 2002, in Proceedings FIR, Submm & mm Detector Technology Workshop, ed. J. Wolf, J. Farhoomand, and C.R. McCreight, NASA/CP-, 211408

Duband L., & Collaudin B., 1999, Cryogenics, 39, 659

Katterloher R., Barl L., Poglitsch A., Royer P., & Stegmaier J., 2006, in Millimeter and Submillimeter Detectors and Instrumentation for Astronomy III, ed. J. Zmuidzinas, W.S. Holland, S. Withington, and W.D. Duncan, Proc. SPIE, 6275, Paper 42

Kraft S., Frenzl O., Charlier O., *et al.*, 2000, in UV, Optical, and IR Space Telescopes and Instruments, ed. J.B. Breckinridge and P. Jakobsen, Proc. SPIE, 4013, 233

Kraft S., Merken P., Creten Y., *et al.*, 2001, in Sensors, Systems, and Next-Generation Satellites V, ed. H. Fujisada, J.B. Lurie, and K. Weber, Proc. SPIE, 4540, 374

Looney L., Raab W., Poglitsch A., & Geis N., 2003, ApJ, 597, 628–643

Poglitsch A., Waelkens C., & Geis N., 1999, in Infrared Spaceborne Remote Sensing VII, ed. M.S. Scholl and B.F. Andresen, Proc. SPIE, 3759, 221

Poglitsch A., Waelkens C., & Geis N., 2003, in IR Space Telescopes and Instruments, ed. J. Mather, Proc. SPIE, 4850, 662

Poglitsch A., Katterloher R., Hönle R., *et al.*, 2003, in Millimeter and Submillimeter Detectors for Astronomy, ed. T. Phillips and J. Zmuidzinas, Proc. SPIE, 4855, 115

Poglitsch A., Waelkens C., Bauer O.H., *et al.*, 2004, in Optical, Infrared, and Millimeter Space Telescopes, ed. J.C. Mather, Proc. SPIE, 5487, 425

Rosenthal D., Beeman J.W., Geis N., *et al.*, 2002, in Proceedings FIR, Submm & mm Detector Technology Workshop, ed. J. Wolf, J. Farhoomand, and C. McCreight, NASA/CP-, 211408

Simoens F., Agnese P., Béguin A., *et al.*, 2004, in Millimeter and Submillimeter Detectors for Astronomy II, ed. J. Zmuidzinas, W.S. Holland, and S. Withington, Proc. SPIE, 5498, 177